ORIGINAL RESEARCH
https://doi.org/10.4209/aaqr.2020.06.0306

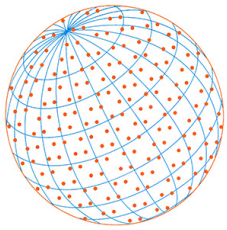

Aerosol and Air Quality Research

Special Issue:
Special Issue on COVID-19 Aerosol Drivers, Impacts and Mitigation (IX)

Impact of COVID-19 Control Measures on Trace Gases (NO_2, HCHO and SO_2) and Aerosols over India during Pre-monsoon of 2020

Mriganka Sekhar Biswas*, D.C. Ayantika

Centre for Climate Change Research, Indian Institute of Tropical Meteorology, Ministry of Earth Sciences, India

ABSTRACT

To prevent the transmission of COVID-19, India implemented country-wide restrictions on socio-economic activities. Using satellite observations for the pre-monsoon (March–April–May) season, we explore the effect of the extended lockdown, on nitrogen dioxide (NO_2), formaldehyde (HCHO), sulfur dioxide (SO_2) and aerosol optical depth (AOD) over India. In this present study we evaluate and quantify the changes in pollutants across six different geographical zones along with the six most populous cities in the country. During April–May the lockdown have resulted in a net decrease in NO_2 column density over India in 2020 compared to 2017–2019 average for the same months. Maximum average seasonal reduction of both NO_2 (–5.6%) and HCHO (–1.3%) occurred over southern India (SI). Compared to March and April, anomalous HCHO for all the regions decreased in May. Anomalous surface cooling induced lower volatile organic carbons (VOCs) emission and slower VOC oxidation due to absence of high nitric oxide led to decrease in HCHO. A reduction in NO_2 was also seen over the top six populous Indian cities, with Mumbai recording the highest decrease (–33.7%). But only Chennai showed a substantial decrease (–6.8%) in HCHO. A significant seasonal reduction in SO_2 was noted over western India (WI) and SI. Additionally, widespread decline covering all the zones was found in the pre-monsoon AOD. In April, the decrease occurred primarily over the Indo-Gangetic-Plains (IGP) and eastern India, while in May a marked homogeneous reduction was noted over entire India. Aerosol induced attenuation of incident solar radiation leads to concurrent changes in MERRA2 insolation during pre-monsoon of 2020. Furthermore, reduced anthropogenic aerosols resulted in reduction of availed cloud condensation nuclei (CCN) leading to larger cloud droplet size and hence increased precipitation during pre-monsoon, 2020.

Keywords: COVID-19, Nitrogen dioxide (NO_2), Formaldehyde (HCHO), Aerosol Optical Depth (AOD), Surface solar radiation

1 INTRODUCTION

Since the first case of COVID-19 was registered in Wuhan, China, in December, 2019 (WHO, 2020a) it has rapidly transmitted across the world by 'SARS-CoV-2'. Till the first week of June, a total of 182 countries and many other territories with confirmed cases of 6,799,713 (WWO, 2020b) have been affected by this novel infectious disease. With WHO declaring COVID-19 as pandemic on 12th March 2020, countries around the world have implemented strict control measures on social and economic activities to prevent the spread of the virus 'SARS-CoV-2' causing COVID-19. India, the second-most populous country in the world, has implemented a nationwide lockdown on 25th March 2020 (https://www.pmindia.gov.in/en/news_updates/pm-calls-for-complete-lockdown-of-entire-nation-for-21-days/; Last access: 08/06/2020). Since then, India has extended the restrictive measures in four stages till 31st May 2020. During this period, except the essential and emergency services; all industrial activities, transport services (road, rail and air), educational institutions, hospitality services, social gatherings, etc., were

OPEN ACCESS

Received: June 11, 2020
Revised: September 6, 2020
Accepted: October 9, 2020

* **Corresponding Author:**
mriganka.cat@tropmet.res.in

Publisher:
Taiwan Association for Aerosol Research
ISSN: 1680-8584 print
ISSN: 2071-1409 online

suspended thereby limiting the movement of 1.3 billion people. The extended control measures on social and economic activities enforced from last week of March to end of May has a direct bearing on the anthropogenically emitted trace gases and aerosols over the Indian subcontinent.

Nitrogen dioxide (NO_2), formaldehyde (HCHO) and sulfur dioxide (SO_2) are among the important trace gases and pollutants having an adverse effect on human health (Burnett *et al.*, 2004; WHO, 2013; Ranzi *et al.*, 2014; Rodriguez-Villamizar *et al.*, 2015; U.S. EPA, 2015; Zhu *et al.*, 2017). While fossil fuel combustion in automobiles and heavy industries, thermal power plants and biomass burning (Stavrakou *et al.*, 2008; Lamsal *et al.*, 2011; Beirle *et al.*, 2003) are the primary sources of anthropogenic NO_2, coal-based thermal power plants and industries are chief emitters of anthropogenic SO_2 (Garg *et al.*, 2001, 2002; Pandey *et al.*, 2014). The formation of HCHO occurs through oxidative degradation of higher volatile organic compounds (VOCs) emitted from biogenic (Fu *et al.*, 2007; Smedt *et al.*, 2010) as well as anthropogenic (Herndon *et al.*, 2005; Zhu *et al.*, 2017) sources. Along with impacting the air quality, these trace gases also play a key role in atmospheric chemistry. NO_2 and HCHO contribute to tropospheric O_3 formation (Crutzen, 1970, 1979; Carter and Atkinson, 1987) and participates in atmospheric redox reaction controlling the oxidative capacity of the atmosphere. NO_2 and SO_2, both are responsible for acid rains (Irwin and Williams, 1988) and acts as aerosol precursors (Seinfeld and Pandis, 2006; Lin and Cheng, 2007).

Over India, along with trace gases, atmospheric aerosols impact local pollution (Mitra and Sharma, 2002; Mönkkönen *et al.*, 2005) while having a profound influence on the regional climate through changes in solar radiation, atmospheric temperature, precipitation processes and the hydrological cycle (Krishnan and Ramanathan, 2002; Ramanathan *et al.*, 2005; Bollasina *et al.*, 2011; Ganguly *et al.*, 2012; Krishnan *et al.*, 2016; Soni *et al.*, 2016). The aerosol concentrations over India are dominated by wind-blown dust, sea salt (natural) and black carbon (BC), organic carbon (OC), sulphate, nitrate produced from urbanization, industrialization, biomass burning, agricultural activities, etc. Substantial contribution of aerosol constituents occurs from industries and thermal power plants, while on-road diesel vehicles are the largest contributor of BC and OC in the transport sector (Reddy and Venkataraman, 2002; Sadavarte and Venkataraman, 2014). The primary source of anthropogenic aerosols over major Indian cities are diesel engine exhaust, gasoline engine exhaust, road dust, coal combustion and biomass combustion (Chowdhury *et al.*, 2007). Interestingly, during the pre-monsoon season (March–April–May), BC, soot and dust accumulate over Indo-Gangetic Plains (IGP), Tibetan Plateau and aids in invigoration on monsoon precipitation (Lau and Kim, 2006; Lau *et al.*, 2006). Additionally, uplifted BC from northern India gets deposited over Himalayan snow and leads to accelerated snowmelt (Lau and Kim, 2010; Kopacz *et al.*, 2011).

In recent decades, emerging India has witnessed rapid growth in population, industrialization, urbanization, which resulted in rising emissions over the region (Ramanathan *et al.*, 2001; Pandey *et al.*, 2014; Sadavarte and Venkataraman, 2014). Using long-term observations an associated increase in NO_2 (Mahajan *et al.*, 2015; Georgoulias *et al.*, 2019), tropospheric HCHO column density (Smedt *et al.*, 2010; Mahajan *et al.*, 2015) and SO_2 column amount (Lu *et al.*, 2013; Qu *et al.*, 2019) has been reported over India. An increase in anthropogenic aerosol loading along with a significant positive trend in aerosol optical depth (AOD) has also been observed over the subcontinent (Satheesh *et al.*, 2017). The recent rising concentrations of atmospheric pollutants over urbanized India is a cause for concern (Guttikunda and Calori, 2013; Gurjar *et al.*, 2016). Along with having consequences on human health (Cohen *et al.*, 2017; Balakrishnan *et al.*, 2019), pollutants impact the radiation balance as well as cloud processes (Ramanathan *et al.*, 2005; Rosenfeld *et al.*, 2008; Vasilkov *et al.*, 2009). In the backdrop of the sustained increase in aerosols and trace gases, the disruption of economic and social activities due to the nationwide lockdown is a unique opportunity to investigate and better recognize the effect of human activity on atmospheric pollutants and aerosols. Over other regions around the world, studies (Devi *et al.*, 2020; Fan *et al.*, 2020; Siciliano *et al.*, 2020; Xu *et al.*, 2020) have noted a reduction in pollution and improvement of air quality during the lockdown period. Recent studies focusing on the early stages of the lockdown studies have reported a decrease in atmospheric pollutants over different regions in the Indian subcontinent (Devara *et al.*, 2020; Jain and Sharma, 2020; Mahato *et al.*, 2020; Sharma *et al.*, 2020). Devara *et al.* (2020) reported an improvement in air quality index in Delhi and nearby region during initial days of COVID-19 induced lockdown (during 25–30 March,

ORIGINAL RESEARCH
https://doi.org/10.4209/aaqr.2020.06.0306

2020). Jain and Sharma (2020) (Jain and Sharma, 2020) reported a decrease in NO_2 concentration by ~51% during 25th March–6th April 2020 compared to 10th–20th March 2020 over Delhi. Mahato *et al.* (2020) reported ~53% and ~18% reduction in NO_2 and SO_2 concentration respectively during 25th March–14th April, 2020 compared to 3rd March–24th March, 2020 in Delhi. Sharma *et al.* (2020) reported overall 18% decrease in NO_2 over India during 16th March–14th, April 2020. Ranjan *et al.* (2020) reported ~45% decrease in AOD over India compared to long term average (2010-2019) during 25th March–15th May, 2020. Metya *et al.* (2020) reported overall ~17% decrease in NO_2 over India in March 2020 compared to 2010-2020 mean. They also reported ~17% decrease in SO_2 over eastern India during lockdown period.

This present study aims to investigate the variations in NO_2, HCHO, SO_2 and AOD distribution over India during the pre-monsoon (March–April–May) 2020, which includes the entire country-wide extended lockdown period of more than two months compared same period during 2017–2019. Unlike the other recent studies over India investigating the effect of COVID-19 induced lockdown which used station data, this study uses satellite observation which helps understanding the large scale spatial changes in trace gases and AOD. We comprehensively analyze and quantify the changes in atmospheric pollutants and aerosols over different zones along with six most populous cities affected by the restricted anthropogenic activities for the complete pre-monsoon season over India.

2 DATA AND METHODOLOGY

2.1 Data

For analysis we have used gridded satellite datasets from two different satellites (i) OMI (Ozone Monitoring Instrument, on board Aura) and (ii) MODIS (Moderate Resolution Imaging Spectroradiometer, on board Terra and Aqua). OMI observations were used for NO_2, HCHO and SO_2. Daily gridded level 3 datasets of NO_2 (OMI-Aura_L3-OMNO2d), HCHO (OMI-Aura_L3-OMHCHOd (González Abad *et al.*, 2015; Sun *et al.*, 2018)) and SO_2 (OMI-Aura_L3-OMSO2e) were downloaded from EARTHDATA portal by NASA (https://acdisc.gesdisc.eosdis.nasa.gov/data/Aura_OMI_Level3/; last access: 03/06/2020). The spatial resolution of NO_2 and SO_2 datasets is 0.25° × 0.25° whereas the spatial resolution of HCHO datasets is 0.1° × 0.1° (Kelly Chance (2019), OMI/Aura Formaldehyde (HCHO) Total Column Daily L3 Weighted Mean Global 0.1 deg Lat/Lon Grid V003, Greenbelt, MD, USA, Goddard Earth Sciences Data and Information Services Center (GES DISC), Accessed: 03/06/2020, https://doi.org/10.5067/Aura/OMI/DATA3010). Daily datasets were temporally averaged to create average monthly datasets. For all NO_2, HCHO and SO_2 datasets, all grid points with negative slant column densities (SCDs) and cloud fraction values lower than 0 and higher than 0.2 were excluded. Grid points representing higher Tibetan plateau and upper Himalayan regions (3000 m above sea level) were not included either. For HCHO, an additional quality control was carried out using 'data flag' parameters available with the data. The grid points with 'data_flag' values higher than 0 were removed.

The AOD analysis is based on observations from MODIS satellite. Monthly averaged level 3 AOD products (MYD08) were downloaded from EARTHDATA portal from NASA (https://ladsweb.modaps.eosdis.nasa.gov/archive/allData/61/MYD08_M3/; last access: 05/06/2020). For the present study we use the merged 550 nm AOD product 'AOD_550_Dark_Target_Deep_Blue_Combined' (Levy *et al.*, 2013). In a recent study Mangla *et al.* (2020) validated this product using ground-based observation over India. They have compared AOD products from MODIS, OMI and MISR satellites with ground-based Aeronet AOD observations over India. The study concluded that the MODIS AOD product showed higher correlation with ground-based observations (R2 = 0.7 at Gandhi college site in IGP region) followed by MISR and OMI. Negative bias for high aerosol loading is less in MODIS products compared MISR and OMI. The data has a 1° × 1° spatial resolution.

Additionally, the Modern-Era Retrospective Analysis for Research and Applications, version-2 (MERRA2) by Gelaro *et al.* (2017) is used to analyze the wind at 850 hPa level, the incident shortwave radiation at surface under clear-sky conditions along with the 2m air temperature. It may be noted that MERRA-2 implements an aerosol assimilation system incorporating ground- and satellite-based aerosol observations (AVHRR, MODIS, MISR, and AERONET) and represents

their interactions with other processes in the weather and climate system (Randles *et al.*, 2017). Integrated Multi-satellitE Retrievals for GPM (IMERG) data was used to study precipitation (https://gpm.nasa.gov/data/imerg; last access: 10/08/2020). IMERG data is derived from observations of GPM satellite constellation (Global Precipitation Measurement). Also, we use the estimated population density data on a 0.25° × 0.25° grid box for the year 2020 from NASA Socioeconomic Data and Applications Center (SEDAC) (CIESIN, 2018).

2.2 Study Region

To understand the impact of country-wide disruption of anthropogenic activity during the pre-monsoon season of 2020, apart from analyzing the spatial-temporal variation of NO_2, HCHO, SO_2 and AOD over the entire Indian landmass, we have divided the Indian region into six sub-regions. (i) North-Eastern India (NEI): comprising seven states of north-eastern India (Arunachal Pradesh, Manipur, Mizoram, Tripura, Meghalaya, Assam, Nagaland), Sikkim and northern West Bengal. This region has higher vegetation density and lower population density. (ii) Central India (CI): covering the states of Madhya Pradesh, Chhattisgarh, Odisha and part of Maharashtra. It is a sparsely populated area with many thermal power plants, steel plants and coal mines within the states of Chhattisgarh and Odisha. Eastern CI has dense forested area. (iii) Southern India (SI): extending over the peninsular part of India consisting of six states (Andhra Pradesh, Telangana, Kerala, Tamil Nadu, Karnataka and Goa). Three out of the six most populous Indian cities are located in SI. Western SI contains forested region in Western Ghats mountain range. (iv) North-Western India (NWI): This is an arid region consisting of Thar Desert and rest of the Rajasthan state. (v) Western India (WI): covering the state of Gujrat and western Maharashtra containing Mumbai and Pune city. This is a highly industrialized region and is the economic hub of India. (vi) Indo Gangetic Plain (IGP): straddled between CI and Himalaya, encompassing states of Punjab, Haryana, Delhi, Uttar Pradesh, Bihar, Jharkhand and southern West Bengal, this region has the highest population density (> 1000 per sq. km.) in India. IGP is also a highly urbanized, industrialized region.

Furthermore, we analyzed the changes in NO_2, HCHO, SO_2 over six most populous cites in India, i.e., Mumbai, Delhi, Kolkata, Chennai, Bangalore and Hyderabad. Spatial data for 1° × 1° grid boxes around the center points of these cities were extracted and averaged to get the representative values from the cities. Fig. 1(a) shows all the six zones and the six cities discussed in this paper. The cities are denoted by 1° × 1° box around them. Fig. 1(b) show the population density over India. The maximum population density can be seen over IGP region. The urban conglomerate regions including the six cities discussed also show high population densities.

2.3 Methodology

The period of study extends over March, April and May of 2020, which is the pre-monsoon or summer season in India and is characterized by the highest seasonal temperature over the subcontinent. Average monthly gridded data of NO_2, HCHO and SO_2 were created from daily gridded data by temporal averaging for March, April and May (MAM) of 2017–2020. For AOD we used the 550 nm monthly MAM AOD for the period 2017–2020. Since the study focuses on relative changes, three-year seasonal average was created using the data for 2017, 2018, 2019 for every month (March, April and May) as well as for the entire pre-monsoon season (March–April–May). Changes in trace gas and AOD are calculated by subtracting the average monthly and seasonal gridded data for the period 2017-2019 from the corresponding data for the year 2020. The percentage changes are computed after spatially averaging the datasets over all the six zones and the six most populous cities. If not otherwise mentioned, the changes (increase/decrease) in trace gas and AOD will indicate the relative changes (increase/decrease) of the corresponding parameter in 2020 compared to its 2017–2019 average value. Recent studies have reported increasing trend of atmospheric NO_2, HCHO and SO_2 over India (discussed in details in the result section). Time averaging (monthly) over longer period (more years) would have reduced the average values for the pollutants due to underlying increasing trend as in the past year the pollutants concentrations were low. Hence the relative changes between time average pollutant concentration and during COVID19 induced lockdown would have led to misleading results. This is the reason for not using monthly average concentration for longer time period (not more than

 https://doi.org/10.4209/aaqr.2020.06.0306

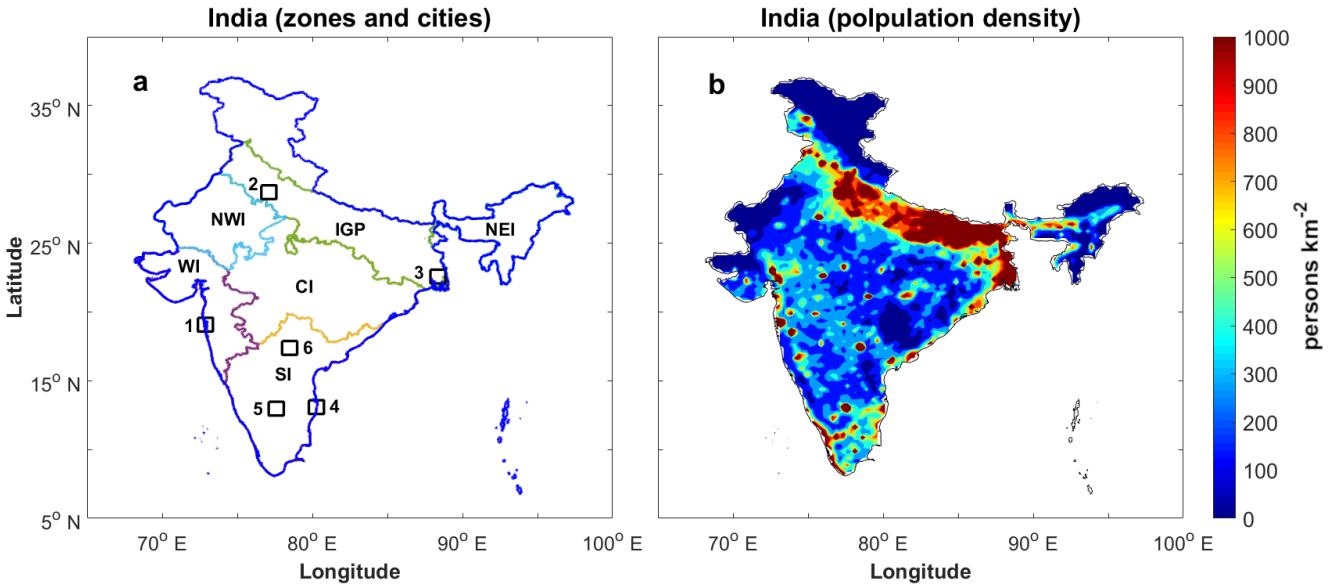

Fig. 1. (a) Map of India with six zones (NEI, CI, SI, NWI, WI and IGP) and six cities. Study areas around the city are marked by the square boxes. Numbering of the cities are as follows: (1) Mumbai, (2) Delhi, (3) Kolkata, (4) Chennai, (5) Bangalore and (6) Hyderabad. (b) Map of population density in India.

three years). Student's t-test was performed to determine statistical significance of the observed changes of mean trace gas concentration and AOD over all the six different geographical region and six different cities in India during 2017–2019 and 2020. In this study we have presented the changes which are statistically significant at 95% confidence interval (p = 0.05) as 'significant'. The changes which are not statistically significant at 95% confidence interval (p = 0.05) are described as 'not significant'.

3 RESULTS AND DISCUSSION

3.1 NO_2

The spatial distribution NO_2 column density over India is plotted in Fig. 2. The mean (2017–2019) NO_2 column density for the pre-monsoon season (Fig. 2(a)) shows high values over IGP, eastern parts of CI and over urban conglomerates (e.g., Mumbai, Bangalore, Chennai). NO_2 hotspot over the Indian capital city of Delhi is prominent in Fig. 2(a). Emission from industries, power plants and automobiles are primary contributors to the high NO_2 concentrations observed over urban conglomerates and industrial regions (Ghude *et al.*, 2008). Another hotspot is observed over the eastern boundary between IGP and CI. Emission from the dual thermal power plants of Rihand (Uttar Pradesh) and Vindhyachal (Madhya Pradesh) generate this hotspot while affecting surface NO_2 concentration in nearby regions (Biswas *et al.*, 2019). The steel plants in the eastern CI and eastern IGP (Bhilai, Raurkela, Durgapur) are also responsible for high tropospheric NO_2 concentrations. The highest average NO_2 column density during MAM of 2017–2019 was found over IGP ($(8.6 \pm 3.0) \times 10^{14}$ molec. cm^{-2}) followed by CI ($(7.6 \pm 2.8) \times 10^{14}$ molec. cm^{-2}). Among the cities, Delhi shows the highest average NO_2 column density ($(11.8 \pm 3.7) \times 10^{14}$ molec. cm^{-2}) during MAM of 2017–2019 followed by Kolkata ($(7.9 \pm 1.2) \times 10^{14}$ molec. cm^{-2}). In the recent decades, satellite observations (OMI, GOME, SCIAMACHY, GOME-2a, 2b) have revealed an increasing trend in tropospheric NO_2 columns over India (Mahajan *et al.*, 2015; Georgoulias *et al.*, 2019). A positive trend in NO_2 is also observed over majority of the Indian cities (Delhi, Kolkata, Chennai, Bengaluru and Hyderabad), while signal over the city of Mumbai is ambiguous (Duncan *et al.*, 2015; Schneider *et al.*, 2015).

Fig. 2(b) shows the changes in NO_2 column density for MAM 2020 with respect to the mean NO_2 column density for MAM 2017–2019. An overall decrease in NO_2 is seen over SI, parts of NEI, eastern IGP and CI. Whereas, over north-western IGP, NWI and parts of WI increase can be seen.

 https://doi.org/10.4209/aaqr.2020.06.0306

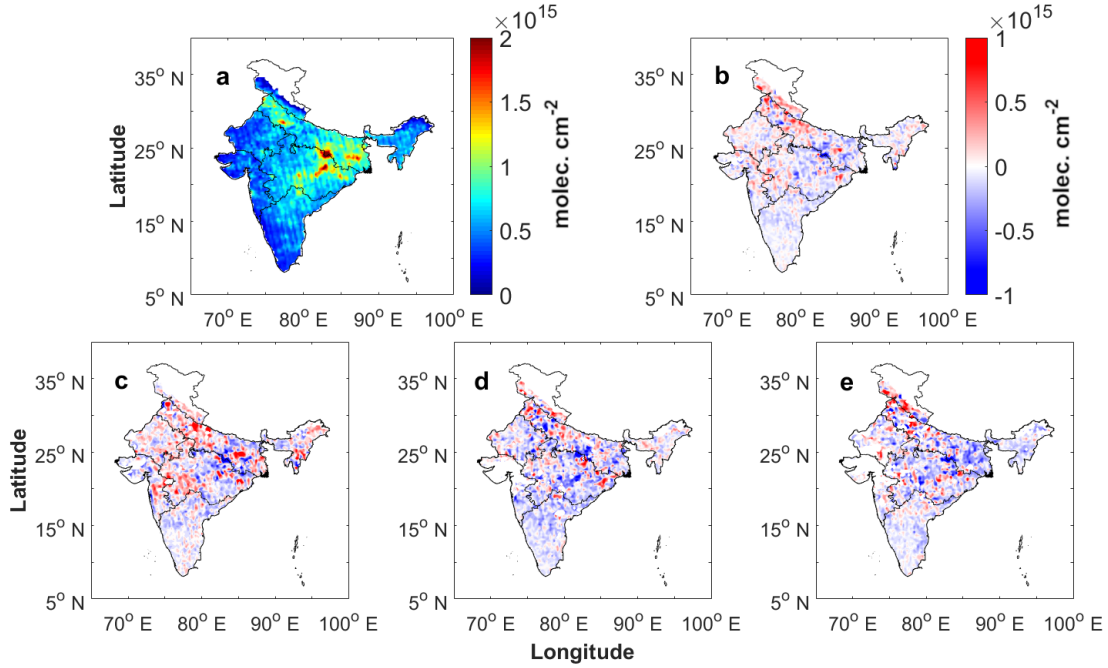

Fig. 2. (a) Spatial distribution of average NO_2 column density during pre-monsoon season of 2017–2019 as observed by OMI satellite. Anomalies of NO_2 column density during (b) pre-monsoon, 2020 (c) March, 2020 (d) April, 2020 (e) May, 2020.

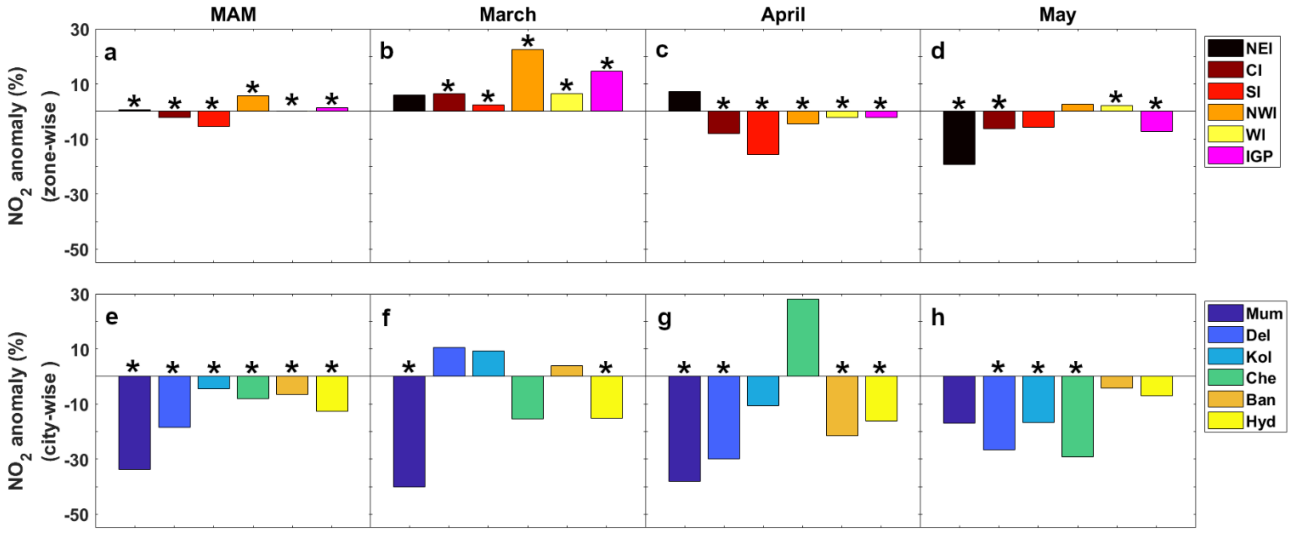

Fig. 3. Percentage changes of zonal average NO_2 column densities over the six Indian zones during (a) pre-monsoon season of 2020 (b) March, 2020, (c) April 2020 and (d) May 2020. Percentage changes of average NO_2 column densities over the six Indian cities during (e) pre-monsoon season of 2020 (f) March, 2020, (g) April 2020 and (h) May 2020. The '*' symbol over the bar plots indicate statistically significant results.

Decrease in NO_2 can be noted over hotspot regions such as Delhi, Rihand – Vindhyachal dual power plants and other urban conglomerates. Fig. 3 shows the zone-wise (Figs. 3(a), 3(b), 3(c) and 3(d)) and city-wise (Figs. 3(e), 3(f), 3(g) and 3(f)) seasonal and monthly percentage changes for pre-monsoon 2020. The '*' over the bar plots in Fig. 3 indicate the statistically significant changes. The MAM, 2020 seasonal percentage change showed decrease over SI and CI. The most substantial decline happened in SI (–5.6%) followed by CI (–2.3%). NWI (+5.8%) showed highest increase during MAM followed by IGP (+1.4%). Fig. 3(e) shows the average percentage changes during the MAM period for all the six cities discussed above. All the six cities have shown negative changes with Mumbai showing the highest decrease (–33.7%) followed by Delhi (–18.5%). The

ORIGINAL RESEARCH
https://doi.org/10.4209/aaqr.2020.06.0306

cumulative percentage changes in NO_2 column density in MAM 2020 compared to MAM 2017–2019 over all the six regions and all the six megacities in India are statistically significant.

Since, the nationwide lockdown in India was enforced on 25th March, 2020, the anthropogenic activities were mostly normal during that month, hence increase in NO_2 column density are observed over all the six zones (Fig. 2(c)) due to underlying increasing trend mentioned earlier. Fig. 3(b) shows the percentage change in NO_2 during March 2020. All the six zones showed increased NO_2 with NWI (+22.5%) showing highest increase followed by IGP (+14.5%) and both the results are statistically significant. During March, Mumbai showed maximum significant decrease (–40%). Delhi recorded highest increase (+10.58%, Fig. 3(f)) but the result is statistically insignificant. Positive changes were also observed over Kolkata and Bangalore. For April 2020, apart from few regions in IGP, NEI and eastern CI the reduction in NO_2 were seen over India (Fig. 1(d)). All the zones except NEI (+7.3% increase) showed an average decrease in NO_2 column density (Fig. 3(c)). However, NEI showed an increase in NO_2, it was found statistically not significant. SI (–15.6%) showed highest significant decrease followed by CI (–8%) in April. During April, only Chennai (+28.07%) showed increase in NO_2 but the result is not statistically significant. All the other cities showed decrease in NO_2 with Mumbai showing maximum significant decrease (–38%) followed by Delhi (–30%, Fig. 3(g)). Fig. 2(e) shows the spatial distribution of NO_2 anomaly over India during May, 2020. Compared to April, the extent of reduction in NO_2 increased during May. The reduction was more pronounced over NEI, eastern IGP and CI with negative changes spreading over more regions (Fig. 2(e)). During May, NEI showed highest significant decrease in NO_2 with –19.3% followed by IGP (–7.2%) region. NWI (+2.7%) and WI (+2.1%) showed positive changes during May, 2020 (Fig. 3(d)) among which only results for WI is statistically significant whereas results for NWI is not statistically significant. During May 2020, all the six major cities showed decrease in NO_2 column density with Chennai showing highest significant decrease (–29.18%) followed by Delhi (–25.37%).

The seasonal average increase of NO_2 column density over WI and IGP was driven by the increase during March. During the 'effective' lockdown period of April and May overall negative departures were observed indicating large decrease in anthropogenic emission and reduction in tropospheric NO_2. Among the six largest Indian cities, Mumbai showed highest significant decrease during MAM (also highest decrease during March and April). This is possibly driven by the underlying negative trend of NO_2 over Mumbai as reported by Duncan *et al.* (2015). The increase of NO_2 column density over Chennai during April is not statistically significant. Unanimous decrease of NO_2 column densities over six cities and the higher decrease over cities compared to the six zones indicate that urban atmosphere is affected more by anthropogenic emission compared to rest of the country. Using this information in chemical model will help to understand and reduce the uncertainty of anthropogenic emission over India better.

3.2 HCHO

Fig. 4 shows the spatial distribution of average HCHO column density and anomalies over India for MAM 2020. Fig. 4(a) represents average HCHO column density for the pre-monsoon period over India during 2017–2019. Three regions show high HCHO column densities (i) the state of Kerala and adjacent region in SI, (ii) the states of Chhattisgarh and Odisha in eastern CI and (iii) NEI region. All these three regions are associated with forests, and biogenic VOCs emitted from these regions get oxidized to produce HCHO (Surl *et al.*, 2018; Chaliyakunnel *et al.*, 2019). Biogenic VOC emissions are dependent on surface temperature and studying positive correlation of HCHO columns with surface temperature Surl *et al.* (2018) inferred that the HCHO variability over India is controlled by biogenic emissions rather than anthropogenic emissions. Apart from these three regions, high HCHO also found over western IGP region of Punjab and Haryana. During pre-monsoon period, crop residue burning happens in Punjab and Haryana leading to pyrogenic emission of VOCs which leads to higher HCHO column density. Pre-monsoon forest fires for converting forest into agricultural lands are also common in NEI (Surl *et al.*, 2018). The highest zonal average during MAM of 2017–2019 was observed over NEI ($(1.5 \pm 0.6) \times 10^{16}$ molec. cm^{-2}) followed by SI ($(1.3 \pm 0.2) \times 10^{16}$ molec. cm^{-2}) and CI ($(1.2 \pm 0.1) \times 10^{16}$ molec. cm^{-2}). Chaliyakunnel *et al.* (2019) estimated that biogenic, anthropogenic and pyrogenic sources are responsible for 44–65%, 37–50% and $< 7\%$ of total VOC emission over India. In two different studies Smedt *et al.* (2010b) and Mahajan *et al.* (2015) reported increasing trend of HCHO over India at 1.3–1.8% yr^{-1}

 https://doi.org/10.4209/aaqr.2020.06.0306

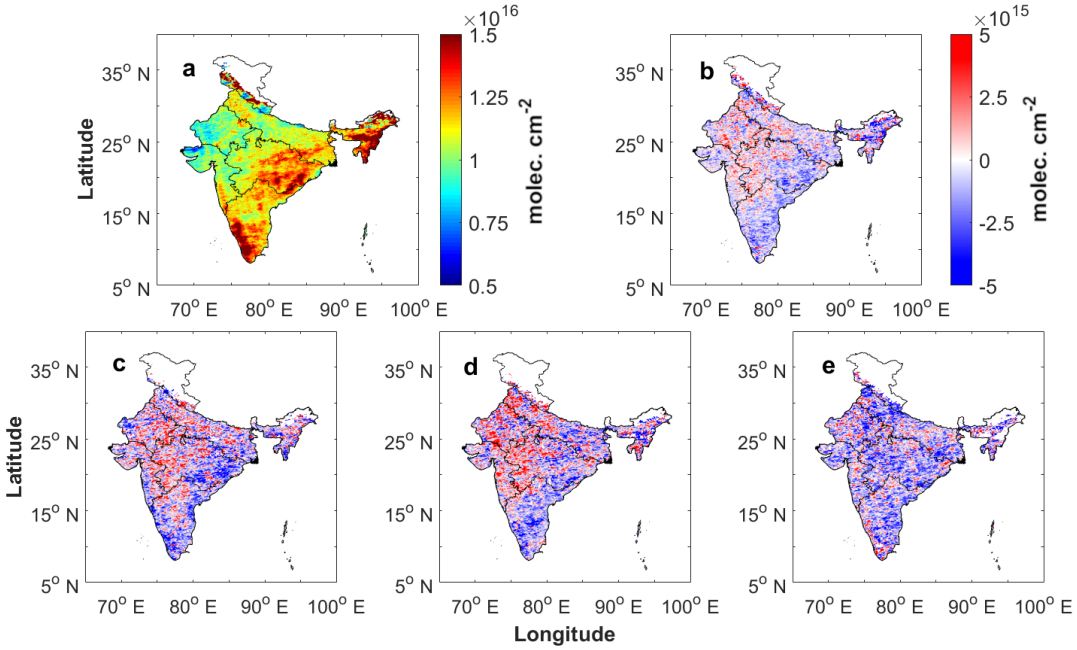

Fig. 4. (a) Spatial distribution of average HCHO column density during pre-monsoon season of 2017–2019 as observed by OMI satellite. Anomalies of HCHO column density during (b) pre-monsoon, 2020 (c) March, 2020 (d) April, 2020 (e) May, 2020.

(for the period 1997–2009) and 1.51 ± 0.44% yr^{-1} (for the period 1995–2013) respectively. Surl *et al.* (2018) reported that anthropogenic VOCs (mainly propene used as solvent) are the major HCHO sources over Indian cities.

Fig. 4(b) shows the average changes of HCHO column density over India during pre-monsoon period. Decrease in HCHO can be seen over the SI, NEI and eastern CI. These are the regions with higher biogenic VOC emission resulting in high HCHO column density. Eastern IGP region also show negative anomaly. Fig. 5 shows the zone-wise and city-wise percentage of HCHO anomalies during pre-monsoon period of 2020. The '*' symbol over the bar plots represent statistically significant results. NEI and SI shows the significant decrease in HCHO column density for overall MAM period with NEI (–2.6% decrease) showing highest decrease followed by SI (–1.3% decrease). NWI (+7.8% increase) recorded the highest significant increase in average HCHO column density followed by WI (+5.0% increase) for pre-monsoon period (Fig. 5(a)). Despite the decrease in HCHO over the forested region of CI, the rest of the CI showed increased HCHO contributing to the net zonal average increase (+3%). Mumbai, Delhi and Hyderabad showed overall increase during MAM 2020 with Hyderabad showing highest increase of +4.8% (Fig. 5(e)). Highest significant reduction was observed over Chennai (–6.8%) for pre-monsoon period of 2020. All the results for changes in HCHO during MAM 2020 over six zone and six cities in India are statistically significant.

Fig. 4(c) shows the HCHO column density anomaly over India during March. SI and eastern CI showed reduction. During March 2020 (Fig. 5(b)), only SI (–2.1%) displayed significant decrease in HCHO column density. Highest increase during March 2020 was observed over NWI (+8.3% increase) followed by WI (+4.8% increase) both the results being statistically significant. Although reduction occurred over east CI, the increase in HCHO column density over west CI caused the zonal average change to be positive over CI (+2.9% increase) being statistically significant. During March (Fig. 5(f)) Mumbai, Kolkata and Chennai showed decrease in HCHO column density, with Chennai showing highest significant decrease (–9.9% decrease). While Kolkata, Bangalore and Hyderabad showed increased HCHO, with Hyderabad showing the highest significant increase (+14.2%) during March.

Fig. 4(d) shows changes in HCHO during April with negative anomaly over SI, eastern CI, eastern IGP and NEI. Despite of decrease in HCHO column density over eastern IGP and eastern CI the average zonal changes over CI and IGP were more positive in April compared to that in March. Also, the average zonal increase over NWI (+12.8% increase) and WI (+9.5% increase) were more

ORIGINAL RESEARCH
https://doi.org/10.4209/aaqr.2020.06.0306

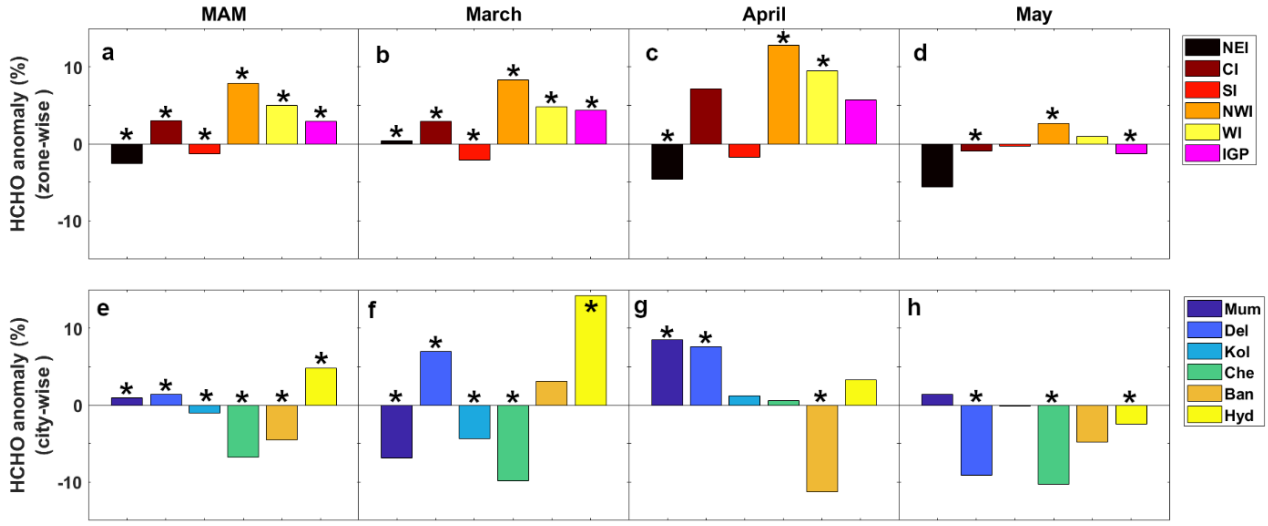

Fig. 5. Percentage changes of zonal average HCHO column densities over the six Indian zones during (a) pre-monsoon season of 2020 (b) March, 2020, (c) April 2020 and (d) May 2020. Percentage changes of average HCHO column densities over the six Indian cities during (e) pre-monsoon season of 2020 (f) March, 2020, (g) April 2020 and (h) May 2020. The '*' symbol over the bar plots indicate statistically significant results.

positive in April compared to March with both the results being statistically significant. Average zonal decrease over NEI (–4.6%, statistically significant) and SI (–1.7%, statistically not significant) were observed during April 2020 (Fig. 5(c)). During April, only Bangalore (–11.3%) showed significant decrease (Fig. 5(g)) whereas all the other cities showed increase with Mumbai showing the highest significant increase (+8.5%).

During May, decrease in HCHO were observed over almost all the six zones (Fig. 4(e)) in patches. Western IGP region over Punjab and Haryana specifically showed decrease in HCHO during May. Except NWI and WI all the other four zones showed zonal average decrease during May with NEI (–5.6%) region showing highest decrease (Fig. 5(d)) followed by IGP (–1.3%). Whereas the result for IGP is statistically significant, the result for NEI is statistically not significant. NWI showed highest significant increase of +2.7%. Compared to March and April, all the zones showed less positive anomaly during May. During May all the cities except Mumbai showed decrease with Chennai (–10.3%) showing highest significant decrease (Fig. 5(h)).

During the March of 2020 HCHO anomalies over the forested regions of SI and CI were mostly negative. In March 2020 there were negative anomalies in surface temperature all over India except SI and NEI (Fig. 10(a)). This negative surface temperature anomaly could lead to lower HCHO column density over eastern CI due to decrease in biogenic VOC emission. In April the negative temperature anomaly appeared all over the India except WI (Fig. 10(b)) which contributed towards reduced HCHO over the forested regions of CI and NEI. Also, the positive temperature anomaly over WI explains the positive anomaly of HCHO over WI in April. In May increase in temperature (Fig. 10(c)) was observed over NWI, WI and SI. This explains the increase in HCHO over NWI and WI. This also explains reduction in HCHO decrease in May compared to April over SI. During March an increase in incoming solar short wave radiation over part of WI and over forested region of CI was observed (Fig. 9(d)). In April the increase in solar short wave radiation over IGP and NWI region could have increased photosynthetic activity with higher VOC emission (Fig. 9(b)). This could cause increase in HCHO over part of WI during March. High increase in solar radiation during April compared to March could further increase HCHO over IGP and NWI region in April compared to March. Biogenic VOCs (isoprene) react to hydroxyl radical (OH) and form peroxy radicals (RO_2). In high NO_x (NO_2 + NO) environment peroxy radicals react with NO and form HCHO along with methyl vinyl ketone (MVK) and methacrolein (MACR). Further oxidation of MVK and MACR by produces more HCHO within few hours. In low NO_x environment, the production of HCHO become slower due to unavailability of NO (Palmer *et al.*, 2006) resulting in reduced the HCHO column density. Due to lockdown effect reduction in NO_2 column (hence reduction in overall NO_X concentration, up to ~100% decrease in places) over SI and eastern CI

and eastern IGP leads to slower oxidation rate of biogenic VOCs resulting in decrease of HCHO column densities in May. In May, due to lockdown effect, less crop residue burning events happened over Punjab and Haryana leading to negative HCHO anomaly. Less number of pre-monsoon forests burning in NEI also could have added to negative HCHO anomaly. However, the decrease in HCHO over SI in March and the increase over NWI (in March) and western CI (during March and April) are not well understood and further research is required. Less emission of anthropogenic VOCs and slower oxidation VOCs in reduced NO_x environment led to decrease in HCHO over all the five cities (except Mumbai) in May. Due to complex interactions between various controlling factors, quantifying the effects of various parameters on HCHO variability during MAM 2020 requires chemistry model-based study.

3.3 SO_2

Fig. 6 represents the spatial distribution of SO_2 column and anomaly over India during MAM, 2020. The mean (2017–2019) spatial distribution of SO_2 column amount (within planetary boundary layer (PBL)) over India is given in Fig. 6(a). The highest values can be found over eastern CI and eastern IGP regions and over major Indian cities due to emissions from thermal power plants, steel plants and automobile emission from cities. The highest seasonal zonal average SO_2 column amount was found over CI (0.2 ± 0.1 D.U.) and IGP (0.2 ± 0.1 D.U.). In two different studies Lu *et al.* (2011, 2013) have reported 71% and 70% increase in SO_2 emission from India during 2005–2012 and 1996–2010 respectively. Qu *et al.* (2019) has used OMI observation products from two different group (NASA and BIRA) and found that SO_2 emission have increased by 35% (NASA product) – 48% (BIRA product) during 2005–2016 over India.

Fig. 6(b) represents the average seasonal changes of SO_2 column amount over India. The positive anomalies are found all over the India. Top panels of Fig. 8 (Figs. 8(a), 8(b), 8(c) and 8(d)) shows the percentage changes of SO_2 during pre-monsoon season of 2020 compared to average for the pre-monsoon of 2017–2019. Statistically significant results are indicated by the '*' symbol over the bar plots. Fig. 8(a) shows the percentage of average seasonal changes of SO_2 during pre-monsoon period over different zones in India. The highest percentage of statistically significant change was found over NWI with +24.7% increase followed by NEI (+5.2% increase). The highest significant decrease was found over WI (–7.3%). All the changes in SO_2 column amount for MAM over six regions in India are statistically significant.

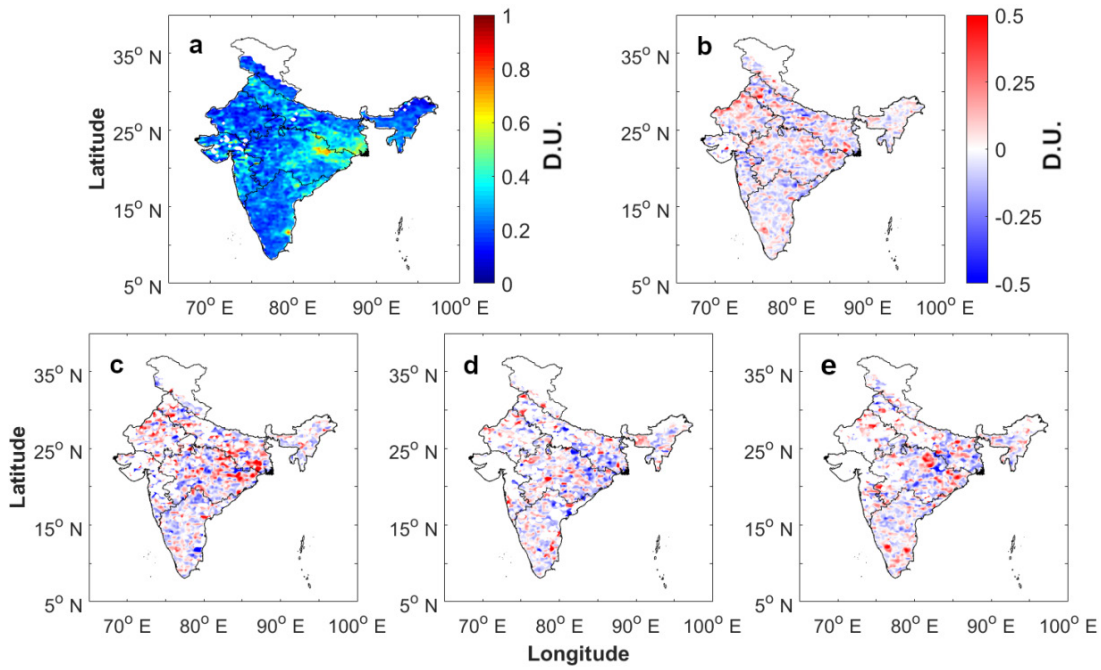

Fig. 6. (a) Spatial distribution of average SO_2 column density during pre-monsoon season of 2017–2019 as observed by OMI satellite. Anomalies of SO_2 column density during (b) pre-monsoon, 2020 (c) March, 2020 (d) April, 2020 (e) May, 2020.

Fig. 6(c) shows the SO_2 anomaly during March, 2020 over India. Increase in SO_2 column amount were found all over the India with large increase in SO_2 were found over parts of CI and NWI. NWI (+32.3%) showed highest significant increase (in percentage) followed by IGP (+13.4%) during March, 2020. WI showed highest significant decrease in average SO_2 column amount of –11.8% during March (Fig. 8(b)). During April (Fig. 6(d)) decrease in SO_2 column amount were found over NEI, eastern CI and eastern IGP region. Decrease over Rihand–Vindhyachal dual power plant region on the border of IGP and CI is very prominent. This is due the reduction of anthropogenic emissions from power plants and heavy industries due to lockdown. NEI (+9.7%) and NWI (+7.2%) are showing zonal average increase (Fig. 8(c)) during April. However, the changes in SO_2 over NEI and NWI in April were statistically not significant. The highest decrease in average zonal anomaly was found over WI region (–11.1%, statistically not significant) followed by IGP region (–8.6%, statistically significant). Decrease in SO_2 column amount were observed over parts of SI, eastern CI and eastern IGP and NEI in May (Fig. 6(e)). The negative anomaly over Kolkata and surrounding places in eastern IGP are visible. NWI showed highest significant increase in SO_2 column amount (Fig. 8(d)) of +28% in May. Only IGP region showed significant decrease in SO_2 by –4.7%.

During the pre-monsoon period of 2020 NWI showed highest significant zonal average positive change of +24.7%. During March and May, NWI consistently showed highest significant increase in zonal average. Whereas IGP showed steady significant decrease in SO_2 during April and May (–8.6% and –4.9%). SI showed decrease in SO_2 March (significant) and April (not significant) whereas in May (not significant) slightly increase. However, NEI showed increase in zonal average SO_2 during April (not significant) and May (significant). Hence lockdown actually reduced the SO_2 concentration over IGP, the most populous region in India. However, the extent of reduction is less compared to that of NO_2 and not unanimous as NO_2. This is due to the fact that major anthropogenic sources of SO_2 emission is from thermal power plants and heavy industries, whereas NO_2 occurs from high temperature combustion processes like automobiles along with power plants and heavy industries.

3.4 AOD

Primarily, aerosol particles absorb and scatter incoming shortwave radiation and AOD is a measure of extinction of solar radiation by these particles. Along with direct emission into the atmosphere (dust, sea salt, soot, organic matter), inorganic and organic aerosols (sulfate, nitrate, ammonium and secondary organic aerosols) are also produced from precursor gases (NO_X, SO_2, ammonia) through atmospheric chemical reactions (Boucher, 2015). Therefore, although AOD represents the columnar content, it can also detect the changes in the lower tropospheric particulate matter under restricted anthropogenic activities (Devi *et al.*, 2020). The pre-monsoon (MAM), seasonal and monthly, 550 nm AOD over India for the year 2020 is analyzed and compared with the mean values of past three years (2017, 2018, 2019) and is shown in Fig. 7. The pre-monsoon mean (2017–2019) AOD (Fig. 7(a).) shows high values ($>$ 0.5) over the IGP region with the maximum burden over the eastern parts. The IGP is characterized by high population density and large aerosol precursor emission sources (David *et al.*, 2018), and is dominated by high concentrations of particulate matter throughout the year (Eck *et al.*, 2010; Ramachandran and Kedia, 2013). During pre-monsoon along with wind-blown dust, fine mode particles comprising of BC and secondary OC from industrial and urban sources contribute to the AOD over the region (Dey *et al.*, 2004; Gautam *et al.*, 2009; Giles *et al.*, 2011; Kedia *et al.*, 2014). High values of AOD are also noticed over western part of NEI, east coast of CI, northeastern region of SI, while a much cleaner environment is noticed over NWI. Intense anthropogenic bio-mass burning and long-range transport from the IGP, Bangladesh regions contribute to the high pre-monsoon aerosol burden over NEI (Kaskaoutis *et al.*, 2014, 2009; Pathak *et al.*, 2016), while the coastal regions are influenced by sea-spray aerosols (Ramachandran and Cherian, 2008). The highest average AOD during MAM of 2017–2019 was found over NEI (0.6 ± 0.2) and IGP region (0.6 ± 0.1).

Fig. 7(b) shows the change in 2020 pre-monsoon 550 nm AOD compared to that of (2017–2019). Interestingly in 2020, a marked reduction of aerosol loading occurs over almost the entire Indian subcontinent, except minor pockets of weak positive anomalies in CI and extreme north NEI. The relative seasonal change in 2020 AOD (in % departures) averaged over different zones (Fig. 8(d)) displays negative change for all zones with IGP, WI, NEI showing –16.5%, –16.0%,

 https://doi.org/10.4209/aaqr.2020.06.0306

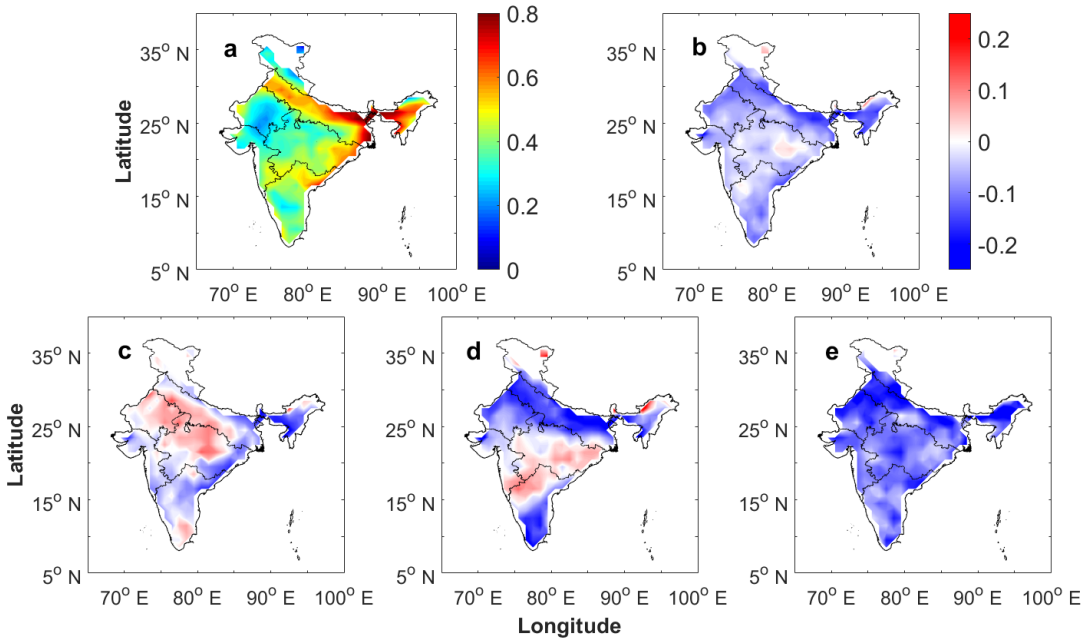

Fig. 7. (a) Spatial distribution of average AOD column density during pre-monsoon season of 2017–2019 as observed by OMI satellite. Anomalies of AOD column density during (b) pre-monsoon, 2020 (c) March, 2020 (d) April, 2020 (e) May, 2020.

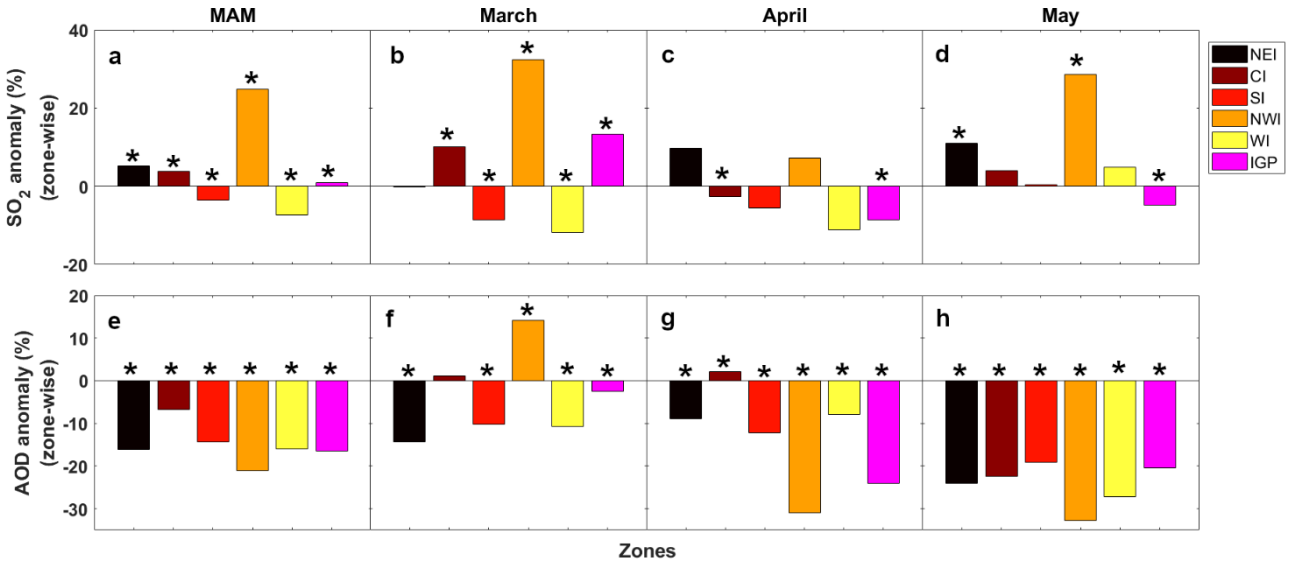

Fig. 8. Percentage changes of zonal average AOD over the six Indian zones during (a) pre-monsoon season of 2020 (b) March, 2020, (c) April 2020 and (d) May 2020. Percentage changes of average SO_2 column amounts over the six Indian zones during (e) pre-monsoon season of 2020 (f) March, 2020, (g) April 2020 and (h) May 2020. The '*' symbol over the bar plots indicate statistically significant results.

–16.0% change respectively with a net decrease of –14.2% (figure not shown) over the Indian landmass. Although considerable year-to-year variability exists in AOD distribution over the subcontinent, such prominent widespread decrease is a distinctive feature of 2020 pre-monsoon season. AOD changes over all six zones in India during MAM 2020 were statistically significant.

On analyzing the change in monthly AOD values, for March 2020 (Fig. 7(c)) we observe an increase in AOD values over parts of northern, central India and the southern tip of the peninsula. Strong reduction occurs over NEI, eastern IGP, coastal Bay of Bengal, and southern peninsula. Marginal reduction is also noticed over Gujrat and western Maharashtra. The maximum significant decrease is seen over NEI (–14.3%; Fig. 8(e)), while significant increase (+14.1%) is observed over

 https://doi.org/10.4209/aaqr.2020.06.0306

NWI. It may be noted that along with local emissions, the AOD over India is affected by long-range transport, atmospheric circulation and other meteorological and geographical factors (Ramachandran and Cherian, 2008; Ramachandran *et al.*, 2012). Since the country-wide control measures over India was in effect from 25th March the changes in AOD in March is mostly due to variations in atmospheric circulation. The 850 mb winds (Fig. 9(a)) shows anomalous south-easterlies over IGP and central India indicating reduced dust transport over northern India. In concurrence with restrictions in various anthropogenic activities the AOD anomalies for April 2020 (Fig. 7(d)) shows a notable decrease over entire northern and eastern India, especially over IGP and NEI. Along with wind-driven dust, local industries, automobile and street dust are major sources of aerosols over the densely populated Indo-Gangetic plains (Dey *et al.*, 2004; Singh *et al.*, 2004). Increase in AOD are seen over CI and northern parts of the southern peninsula. The low level circulation change for April 2020 (Fig. 9(b)) do not reflect large changes in horizontal winds over IGP and eastern India indicating that the decrease in AOD's over this region was primarily due to reduction in anthropogenic emissions. Whereas over parts of CI and peninsular India anomalous easterlies suggest import of natural aerosols from Bay of Bengal. From Fig. 8(f) we can see that the maximum significant decrease in aerosol loading for the month of April occurs over NWI (–31.0%) followed by IGP (–24.0%). Strikingly, in response to the extended control measures, the AOD anomalies for May 2020 (Fig. 7(e)) shows an extensive homogenous reduction in aerosol loading over the entire country. The maximum decrease coincides with the location of major urban-industrial cities in northern IGP. The average changes for all the six zones (Fig. 8(g)) shows decrease in AOD with –32.7%, –20.4%, –24.0%, –22.5%, –27.2%, –19.2% change over NWI, IGP, NEI, CI, WI and SI respectively with results from all the zones being statistically significant. The 850mb circulation change for the month of May 2020 (Fig. 9(c)) shows easterly anomalies over peninsular India with no significant change over northern India. Therefore, the substantial decrease in AOD is largely caused by the cutback in anthropogenically emitted fine particles, mostly BC, OC, sulphate, and would directly impact the incoming solar radiation reaching surface thus altering the surface radiation balance (Ramanathan *et al.*, 2001).

On comparing MERRA2 clear-sky incoming shortwave radiation for March, April and May 2020 (Figs. 9(d), 9(e) and 9(f) respectively) with the average values for (2017–2019) we notice a striking resemblance with the change in AOD patterns for the respective months. For all the three months we notice that decrease (increase) in AOD are coincident with increased (decreased) solar radiation at the surface. In April 2020, in response to diminished aerosol scattering/absorption a considerable increase in insolation (> 5 W m^{-2}) is observed across IGP. Elevated levels are also

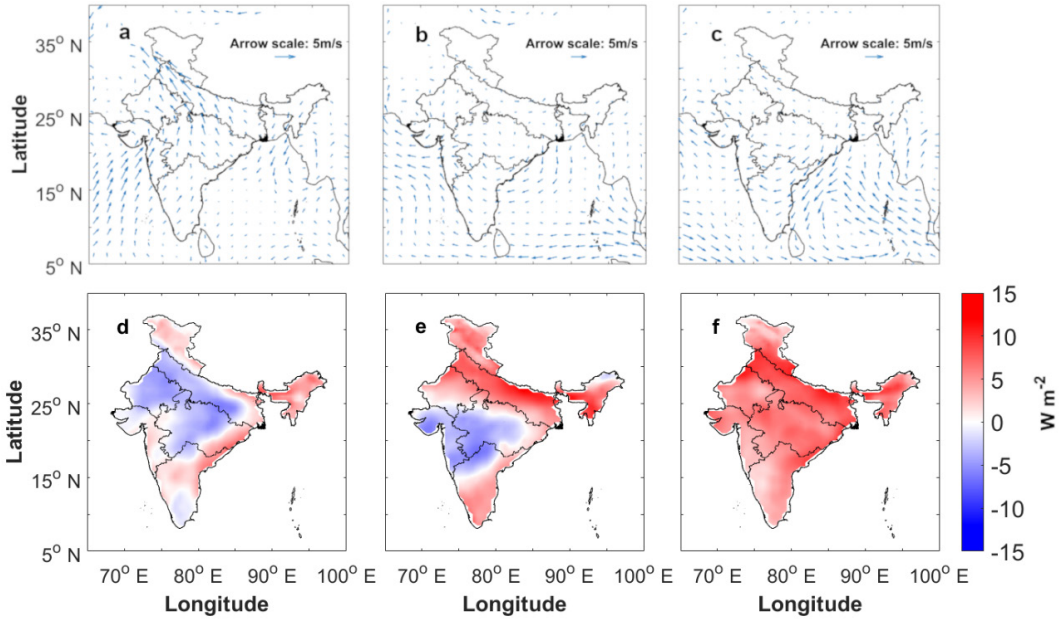

Fig. 9. MERRA2 850 hPa wind anomaly during (a) March, (b) April and (c) May 2020. MERRA2 incoming clear-sky shortwave radiation anomaly during (d) March, (e) April and (f) May 2020.

 https://doi.org/10.4209/aaqr.2020.06.0306

seen over eastern, southern and northwest India. Homogenous increase insolation across the entire Indian subcontinent is observed. Additionally, on analyzing the MERRA2 2 m temperature changes for March, April and May 2020 (Figs. 10(a), 10(b) and 10(c) respectively) with respect to the long-term (1980–2009) monthly climatology, we observe profound cooling north of 15°N in March 2020. In April and May although more radiation was available due to reduced aerosol concentrations, the temperature changes showed cooling across northern, central and eastern India. Different meteorological fields influence the surface temperatures during the pre-monsoon season. Along with aerosol loading, changes in precipitation have a major impact on the MAM surface temperatures. Using IMERG data we have studied the changes in precipitation during March, April and May of 2020 compared to the average precipitation during MAM of 2017–2019 over India (Fig. 10(d), 10(e), and 10(f) respectively). Enhanced rainfall activity due to higher incidences of thunderstorms, western disturbances and a very severe cyclonic storm led to the cool surface temperatures in the 2020 pre-monsoon months. Sinha *et al.* (2019) reported that increase in aerosol loading from industrial emission have resulted in increased available cloud condensation nuclei (CCN) during pre-monsoon season over India. In presence of high available CCN concentration, cloud droplets get reduced in size resulting in delayed onset of collision and coalescence in cloud eventually leading to reduced precipitation. Hence the increased pre-monsoon rainfall was an effect of reduced aerosol loading in MAM 2020 (as evidenced from reduction in AOD).

4 CONCLUSIONS

In this study, satellite observations of NO_2, HCHO, SO_2 (OMI) and 550 nm AOD (MODIS) for the pre-monsoon period (March, April and May) of 2020 were analyzed and compared with that of (2017–2019) pre-monsoon season to evaluate the changes in trace gases and aerosol loading due to restrictions in human activities. Reduction in anthropogenic emissions resulted in reduced seasonal average NO_2 column densities over four zones of NEI, CI, SI and WI with highest decrease over SI (–5.6%). Compared to March 2020, when all the six zones in India showed positive anomalies, implementation of nationwide lockdown resulted in reduced average NO_2 column densities over all the six zones in April and May. The overall increase in seasonal average NO_2 column density over NWI and IGP was driven by higher increase in March 2020. A unanimous substantial decrease of seasonal and monthly average (for May 2020) NO_2 column densities over

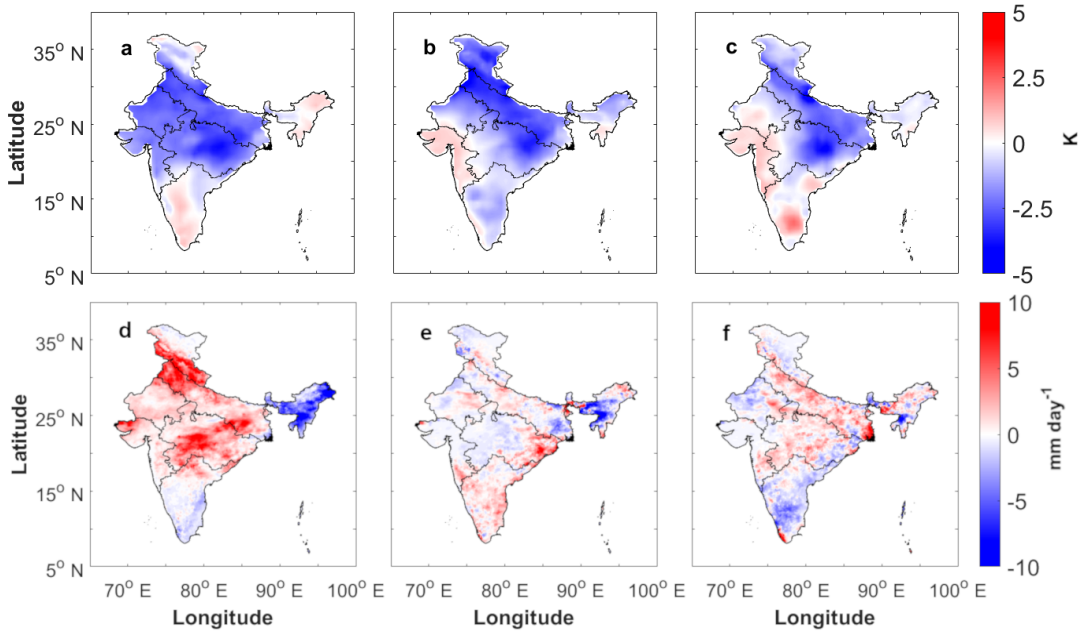

Fig. 10. MERRA2 2 meter temperature anomaly during (a) March, (b) April and (c) May 2020. IMERG precipitation anomaly during (d) March, (e) April and (f) May 2020.

all the six most populous cities in India compared to the six zones indicate that anthropogenic activities drive NO_2 (and other pollutant) concentrations over urban conglomerate compared to rest of the India. Only two zones (NEI and SI) showed decrease in average HCHO column densities during pre-monsoon season of 2020 with SI showing highest decrease (–1.3%). However, during May 2020, NEI, CI, SI and IGP showed negative anomalies (highest significant decrease over IGP, –1.3%), whereas HCHO anomaly over NWI and WI also decreased compared to March and April. Decrease in HCHO column densities were result of reduction in biogenic, VOC emission due to decrease in surface temperature. Reduction in anthropogenic and pyrogenic (over NEI and western IGP) VOC emission added to decrease in HCHO column densities. Also, the reduction in VOC oxidation rate due to decrease in NO_X concentration at places with normally high NO_2 concentrations resulted in decreased HCHO column height. Lower emission of anthropogenic VOCs and slower oxidation VOCs in reduced NO_X environment resulted in reduction of HCHO column density over all the five cities (except Mumbai) during may, 2020. IGP regions showed significant decrease in zonal average SO_2 column amount during April and May. Whereas NWI region showed continuous positive anomaly over the pre-monsoon season. This indicates that lockdown period reduced the relative SO_2 concentration over IGP by reducing anthropogenic emissions.

The change in AOD during the 2020 pre-monsoon season shows large-scale decrease spanning almost the entire Indian landmass. Monthly variations indicate increased aerosol loading over north, central and south India for March 2020, caused by the deviations in meteorological conditions. In April, with the implementation of control measures, a major reduction in aerosols occurs along the highly populated industrial IGP region (–24.0%). Remarkably in May 2020, the AOD change shows a harmonized decrease over all the regions (IGP: –20.4%, NEI: –24.0%, CI: –22.5%, WI: –27.2%, SI: –19.2%, NWI: –32.7%). The direct impact of the AOD change is observed in the incident shortwave radiation at the surface. Decreased anthropogenic aerosol loading leads to lower attenuation of solar radiation, thus increasing the available energy at the surface. In contrast, the surface temperature change for the pre-monsoon months of 2020 shows negative anomalies over the north, central and east India. This anomalous surface cooling is connected to the enhanced pre-monsoon rain events occurring over the country in pre-monsoon 2020. As is well known, the interaction of aerosols and clouds is a highly complex and uncertain scientific problem (IPCC, 2013; Fadnavis *et al.*, 2020). Hence along with evaluating air-quality for pollution mitigation policy, the COVID-19 restrictive environment can be used to study the challenging issue of aerosol-precipitation-meteorology interaction.

ACKNOWLEDGMENTS

The authors thank Director, Indian Institute of Tropical Meteorology (IITM), Pune for his support and encouragement. IITM receives full support from the Ministry of Earth Sciences, Government of India. The author also thanks Ms. Debotri Roy for helping with statistical analysis.

REFERENCES

Balakrishnan, K., Dey, S., Gupta, T., Dhaliwal, R.S., Brauer, M., Cohen, A.J., Stanaway, J.D., Beig, G., Joshi, T.K., Aggarwal, A.N., Sabde, Y., Sadhu, H., Frostad, J., Causey, K., Godwin, W., Shukla, D.K., Kumar, G.A., Varghese, C.M., Muraleedharan, P., … Dandona, L. (2019). The impact of air pollution on deaths, disease burden, and life expectancy across the states of India: The Global Burden of Disease Study 2017. Lancet Planetary Health 3, e26–e39. https://doi.org/10.1016/S2542-5196(18)30261-4

Beirle, S., Platt, U., Wenig, M., Wagner, T. (2003). Weekly cycle of NO_2 by GOME measurements: A signature of anthropogenic sources. Atmos. Chem. Phys. 3, 2225–2232. https://doi.org/10.5194/acp-3-2225-2003

Biswas, M.S., Ghude, S.D., Gurnale, D., Prabhakaran, T., Mahajan, A.S. (2019). Simultaneous observations of nitrogen dioxide, formaldehyde and ozone in the Indo-Gangetic Plain. Aerosol Air Qual. Res. 19, 1749–1764. https://doi.org/10.4209/aaqr.2018.12.0484

Bollasina, M.A., Ming, Y., Ramaswamy, V. (2011). Anthropogenic aerosols and the weakening of

the south asian summer monsoon. Science 334, 502–505. https://doi.org/10.1126/science.1204994

Boucher, O. (2015). Atmospheric aerosols properties and climate impacts. Springer Netherlands. https://doi.org/10.1007/978-94-017-9649-1

Burnett, R.T., Stieb, D., Brook, J.R., Cakmak, S., Dales, R., Raizenne, M., Vincent, R., Dann, T. (2004). Associations between short-term changes in nitrogen dioxide and mortality in Canadian cities. Arch. Environ. Health 59, 228–36. https://doi.org/10.3200/AEOH.59.5.228-236

Carter, W.P.L., Atkinson, R. (1987). An experimental study of incremental hydrocarbon reactivity. Environ. Sci. Technol. 21, 67–679. https://doi.org/10.1021/es00161a008

Chaliyakunnel, S., Millet, D.B., Chen, X. (2019). Constraining emissions of volatile organic compounds over the Indian Subcontinent using space-based formaldehyde measurements. J. Geophys. Res. 124, 10525–10545. https://doi.org/10.1029/2019JD031262

Chowdhury, Z., Zheng, M., Schauer, J.J., Sheesley, R.J., Salmon, L.G., Cass, G.R., Russell, A.G. (2007). Speciation of ambient fine organic carbon particles and source apportionment of $PM_{2.5}$ in Indian cities. J. Geophys. Res. 112, D15303. https://doi.org/10.1029/2007JD008386

CIESIN (2018). Gridded Population of the World, Version 4 (GPWv4): Population Density Adjusted to Match 2015 Revision UN WPP Country Totals, Revision 11. Palisades, NY.

Cohen, A.J., Brauer, M., Burnett, R., Anderson, H.R., Frostad, J., Estep, K., Balakrishnan, K., Brunekreef, B., Dandona, L., Dandona, R., Feigin, V., Freedman, G., Hubbell, B., Jobling, A., Kan, P.H., Knibbs, L., Liu, Y., Martin, P.R., Morawska, L., … Forouzanfar, M.H. (2017). Estimates and 25-year trends of the global burden of disease attributable to ambient air pollution: An analysis of data from the Global Burden of Diseases Study 2015. Lancet 389, 1907–1918. https://doi.org/10.1016/S0140-6736(17)30505-6

Crutzen, P.J. (1970). The influence of nitrogen oxides on the atmospheric ozone content. Q. J. R. Meteorolog. Soc. 96, 320–325. https://doi.org/10.1002/qj.49709640815

Crutzen, P.J. (1979). The Role of NO and NO_2 in the chemistry of the troposphere and stratosphere. Annu. Rev. Earth Planet. Sci. 7, 443–472. https://doi.org/10.1146/annurev.ea.07.050179.002303

David, L.M., Ravishankara, A.R., Kodros, J.K., Venkataraman, C., Sadavarte, P., Pierce, J.R., Chaliyakunnel, S., Millet, D.B. (2018). Aerosol optical depth over India. J. Geophys. Res. 123, 3688–3703. https://doi.org/10.1002/2017JD027719

Devara, P., Kumar, A., Sharma, P.B., Banerjee, P., Khan, A.A., Tripathi, A., Tiwari, S., Beig, G. (2020). Influence of Air Pollution on Coronavirus (COVID-19): Some Evidences from Studies at AUH, Gurugram, India. SSRN. http://.doi.org/10.2139/ssrn.3588060

Dey, S., Tripathi, S.N., Singh, R.P., Holben, B.N. (2004). Influence of dust storms on the aerosol optical properties over the Indo-Gangetic basin. J. Geophys. Res. 109, D20211. https://doi.org/10.1029/2004JD004924

Duncan, B.N., Lamsal, L.N., Thompson, A.M., Yoshida, Y., Lu, Z., Streets, D.G., Hurwitz, M.M., Pickering, K.E. (2015). A space-based, high-resolution view of notable changes in urban NO_x pollution around the world (2005-2014). J. Geophys. Res. 120, 976–996. https://doi.org/10.1002/2015JD024121

Eck, T.F., Holben, B.N., Sinyuk, A., Pinker, R.T., Goloub, P., Chen, H., Chatenet, B., Li, Z., Singh, R.P., Tripathi, S.N., Reid, J.S., Giles, D.M., Dubovik, O., Neill, N.T.O., Smirnov, A., Wang, P., Xia, X. (2010). Climatological aspects of the optical properties of fine/coarse mode aerosol mixtures. J. Geophys. Res. 115, D19205. https://doi.org/10.1029/2010JD014002

Fadnavis, S., Mahajan, A.S., Choudhury, A.D., Roy, C., Singh, M., Biswas, M.S., Pandithurai, G., Prabhakaran, T., Lal, S., Venkatraman, C., Ganguly, D., Sinha, V., Sarin, M.M. (2020). Atmospheric aerosols and trace gases, in: Krishnan, R., Sanjay, J., Gnanaseelan, C., Mujumdar, M., Kulkarni, A., Chakraborty, S. (Eds)., Assessment of climate change over the Indian Region, Springer, Singapore, pp. 93–116. https://doi.org/10.1007/978-981-15-4327-2_5

Fan, C., Li, Y., Guang, J., Li, Z., Elnashar, A., Allam, M., de Leeuw, G. (2020). The impact of the control measures during the COVID-19 outbreak on air pollution in China. Remote Sens. 12, 1613. https://doi.org/10.3390/rs12101613

Fu, T.M., Jacob, D.J., Palmer, P.I., Chance, K., Wang, Y.X., Barletta, B., Blake, D.R., Stanton, J.C., Pilling, M.J. (2007). Space-based formaldehyde measurements as constraints on volatile organic compound emissions in east and south Asia and implications for ozone. J. Geophys.

Res. 112, D06312. https://doi.org/10.1029/2006JD007853
Ganguly, D., Rasch, P.J., Wang, H., Yoon, J.H. (2012). Climate response of the South Asian monsoon system to anthropogenic aerosols. J. Geophys. Res. 117, D13209. https://doi.org/10.1029/2012JD017508
Garg, A., Shukla, P.R., Bhattacharya, S., Dadhwal, V.K. (2001). Sub-region (district) and sector level SO_2 and NO_2 emissions for India: Assessment of inventories and mitigation exibility. Atmos. Environ. 35, 703–713. https://doi.org/10.1016/S1352-2310(00)00316-2
Garg, A., Kapshe, M., Shukla, P.R., Ghosh, D. (2002). Large point source (LPS) emissions from India: Regional and sectoral analysis. Atmos. Environ. 36, 213–224. https://doi.org/10.1016/S1352-2310(01)00439-3
Gautam, R., Hsu, N.C., Lau, K.M., Kafatos, M. (2009). Aerosol and rainfall variability over the Indian monsoon region: Distributions ,trends and coupling. Ann. Geophys. 27, 3691–3703. https://doi.org/10.5194/angeo-27-3691-2009
Gelaro, R., McCarthy, W., Suárez, M.J., Todling, R., Molod, A., Takacs, L., Randles, C., Darmenov, A., Bosilovich, M.G., Reichle, R., Wargan, K., Coy, L., Cullather, R., Draper, C., Akella, S., Buchard, V., Conaty, A., da Silva, A., Gu, W., … Zhao, B, (2017). The modern-era retrospective analysis for research and applications, version 2 (MERRA-2). J. Clim. 30, 5419–5454. https://doi.org/10.1175/JCLI-D-16-0758.1
Georgoulias, A.K., van der A, R.J., Stammes, P., Boersma, K.F., Eskes, H.J. (2019). Trends and trend reversal detection in 2 decades of tropospheric NO_2 satellite observations. Atmos. Chem. Phys. 19, 6269–629. https://doi.org/10.5194/acp-19-6269-2019
Ghude, S.D., Fadnavis, S., Beig, G., Polade, S.D., van der A, R.J. (2008). Detection of surface emission hot spots, trends, and seasonal cycle from satellite-retrieved NO_2 over India. J. Geophys. Res. 113, D20305. https://doi.org/10.1029/2007JD009615
Giles, D.M., Holben, B.N., Tripathi, S.N., Eck, T.F., Newcomb, W.W., Slutsker, I., Dickerson, R.R., Thompson, A.M., Mattoo, S., Wang, S.H., Singh, R.P., Sinyuk, A., Schafer, J.S. (2011). Aerosol properties over the Indo-Gangetic Plain: A mesoscale perspective from the TIGERZ experiment. J. Geophys. Res. 116, D18203. https://doi.org/10.1029/2011JD015809
González Abad, G., Liu, X., Chance, K., Wang, H., Kurosu, T.P., Suleiman, R. (2015). Updated Smithsonian Astrophysical Observatory Ozone Monitoring Instrument (SAO OMI) formaldehyde retrieval. Atmos. Meas. Tech. 8, 19–32. https://doi.org/10.5194/amt-8-19-2015
Gurjar, B.R., Ravindra, K., Singh, A. (2016). Air pollution trends over Indian megacities and their local-to-global implications. Atmos. Environ. 142, 475–495. https://doi.org/10.1016/j.atmosenv.2016.06.030
Guttikunda, S.K., Calori, G. (2013). A GIS based emissions inventory at 1 km × 1 km spatial resolution for air pollution analysis in Delhi, India. Atmos. Environ. 67, 101–111. https://doi.org/10.1016/j.atmosenv.2012.10.040
Herndon, S.C., Jayne, J.T., Zahniser, M.S., Worsnop, D.R., Knighton, B., Alwine, E., Lamb, B.K., Zavale, M., Nelson, D.D., McManus, J.B., Shorter, J.H., Canagaratna, M.R., Onasch, T.B., Kolb, C.E. (2005). Characterization of urban pollutant emission fluxes and ambient concentration distributions using a mobile laboratory with rapid response instrumentation. Faraday Discuss. 130, 327–339. https://doi.org/10.1039/B500411J
IPCC (2013). Fifth assessment report of the intergovernmental panel on climate change (IPCC).
Irwin, J.G., Williams, M.L. (1988). Acid rain: Chemistry and transport. Environ. Pollut. 50, 29–59. https://doi.org/10.1016/0269-7491(88)90184-4
Jain, S., Sharma, T. (2020). Social and travel lockdown impact considering coronavirus disease (COVID-19) on air quality in megacities of India: Present benefits, future challenges and way forward. Aerosol Air Qual. Res. 20, 1222–1236. https://doi.org/10.4209/aaqr.2020.04.0171
Kanniah, K.D., Kamarul Zaman, N.A., Kaskaoutis, D.G., Latif, M.T. (2020). Science of the Total Environment COVID-19's impact on the atmospheric environment in the Southeast Asia region. Sci. Total Environ. 736, 139658. https://doi.org/10.1016/j.scitotenv.2020.139658
Kaskaoutis, D.G., Badarinath, K.V.S., Kharol, S.K., Sharma, A.R., Kambezidis, H.D. (2009). Variations in the aerosol optical properties and types over the tropical urban site of Hyderabad, India. J. Geophys. Res. 114, D22204. https://doi.org/10.1029/2009JD012423
Kaskaoutis, D.G., Kumar, S., Sharma, D., Singh, R.P., Kharol, S.K., Sharma, M., Singh, A.K., Singh, S., Singh, A., Singh, D. (2014). Effects ofcrop residue burningonaerosol properties, plume

characteristics, and long-range transport over northern India. J. Geophys. Res. 119, 5424–5444. https://doi.org/10.1002/2013JD021357

Kedia, S., Ramachandran, S., Holben, B.N., Tripathi, S.N. (2014). Quantification of aerosol type , and sources of aerosols over the Indo-Gangetic Plain. Atmos. Environ. 98, 607–619. https://doi.org/10.1016/j.atmosenv.2014.09.022

Kopacz, M., Mauzerall, D.L., Wang, J., Leibensperger, E.M., Henze, D.K., Singh, K., Sciences, A., Science, A. (2011). Origin and radiative forcing of black carbon transported to the Himalayas and Tibetan Plateau. Atmos. Chem. Phys. 11, 2837–2852. https://doi.org/10.5194/acp-11-2837-2011

Krishnan, R., Ramanathan, V. (2002). Evidence of surface cooling from absorbing aerosols. Geophys. Res. Lett. 29, 54-1–54-4. https://doi.org/10.1029/2002GL014687

Krishnan, R., Sabin, T.P., Vellore, R., Mujumdar, M., Sanjay, J., Goswami, B.N., Hourdin, F., Dufresne, J.L., Terray, P. (2016). Deciphering the desiccation trend of the South Asian monsoon hydroclimate in a warming world. Clim. Dyn. 47, 1007–1027. https://doi.org/10.1007/s00382-015-2886-5

Lamsal, L.N., Martin, R.V., Padmanabhan, A., van Donkelaar, A., Zhang, Q., Sioris, C.E., Chance, K., Kurosu, T.P., Newchurch, M.J. (2011). Application of satellite observations for timely updates to global anthropogenic NO_x emission inventories. Geophys. Res. Lett. 38, L05810. https://doi.org/10.1029/2010GL046476

Lau, K., Kim, K. (2006). Observational relationships between aerosol and Asian monsoon rainfall, and circulation. Geophys. Res. Lett. 33, L21810. https://doi.org/10.1029/2006GL027546

Lau, K.M., Kim, M.K., Kim, K.M. (2006). Asian summer monsoon anomalies induced by aerosol direct forcing: The role of the Tibetan Plateau. Clim. Dyn. 26, 855–864. https://doi.org/10.1007/s00382-006-0114-z

Lau, W.K.M., Kim, K.M. (2010). Fingerprinting the impacts of aerosols on long-term trends of the Indian summer monsoon regional rainfall. Geophys. Res. Lett. 37, L16705. https://doi.org/10.1029/2010GL043255

Levy, R.C., Mattoo, S., Munchak, L.A., Remer, L.A., Sayer, A.M., Patadia, F., Hsu, N.C. (2013). The Collection 6 MODIS aerosol products over land and ocean. Atmos. Meas. Tech. 6, 2989–3034. https://doi.org/10.5194/amt-6-2989-2013

Lin, Y.C., Cheng, M.T. (2007). Evaluation of formation rates of NO_2 to gaseous and particulate nitrate in the urban atmosphere. Atmos. Environ. 41, 1903–1910. https://doi.org/10.1016/j.atmosenv.2006.10.065

Lu, Z., Zhang, Q., Streets, D.G. (2011). Sulfur dioxide and primary carbonaceous aerosol emissions in China and India, 1996-2010. Atmos. Chem. Phys. 11, 9839–9864. https://doi.org/10.5194/acp-11-9839-2011

Lu, Z., Streets, D.G., de Foy, B., Krotkov, N.A. (2013). Ozone monitoring instrument observations of interannual increases in SO_2 emissions from Indian coal-fired power plants during 2005-2012. Environ. Sci. Technol. 47, 13993–14000. https://doi.org/10.1021/es4039648

Mahajan, A.S., De Smedt, I., Biswas, M.S., Ghude, S., Fadnavis, S., Roy, C., van Roozendael, M. (2015). Inter-annual variations in satellite observations of nitrogen dioxide and formaldehyde over India. Atmos. Environ. 116, 194–201. https://doi.org/10.1016/j.atmosenv.2015.06.004

Mahato, S., Pal, S., Ghosh, K.G. (2020). Effect of lockdown amid COVID-19 pandemic on air quality of the megacity Delhi, India. Sci. Total Environ. 730, 139086. https://doi.org/10.1016/j.scitotenv.2020.139086

Mangla, R., Indu, J., Chakra, S.S. (2020). Inter-comparison of multi-satellites and Aeronet AOD over Indian Region. Atmos. Res. 240, 104950. https://doi.org/10.1016/j.atmosres.2020.104950

Metya, A., Dagupta, P., Halder, S., Chakraborty, S., Tiwari, Y.K. (2020). COVID-19 lockdowns improve air quality in the South-East Asian regions, as seen by the remote sensing satellites. Aerosol Air Qual. Res. 20, 1772–1782. https://doi.org/10.4209/aaqr.2020.05.0240

Mitra, A.P., Sharma, C. (2002). Indian aerosols: Present status. Chemosphere 49, 1175–1190. https://doi.org/10.1016/S0045-6535(02)00247-3

Mönkkönen, P., Koponen, I.K., Lehtinen, K.E.J., Hämeri, K., Uma, R., Kulmala, M. (2005). Measurements in a highly polluted Asian mega city: Observations of aerosol number size distribution, modal parameters and nucleation events. Atmos. Chem. Phys. 5, 57–66. https://doi.org/10.5194/acp-5-57-2005

Palmer, P.I., Abbot, D.S., Fu, T.M., Jacob, D.J., Chance, K., Kurosu, T.P., Guenther, A., Wiedinmyer, C., Stanton, J.C., Pilling, M.J., Pressley, S.N., Lamb, B., Sumner, A.L. (2006). Quantifying the seasonal and interannual variability of North American isoprene emissions using satellite observations of the formaldehyde column. J. Geophys. Res. 111, D12315. https://doi.org/10.1029/2005JD006689

Pandey, A., Sadavarte, P., Rao, A.B., Venkataraman, C. (2014). Trends in multi-pollutant emissions from a technology-linked inventory for India: II. Residential, agricultural and informal industry sectors. Atmos. Environ. 99, 341–352. https://doi.org/10.1016/j.atmosenv.2014.09.080

Pathak, B., Subba, T., Dahutia, P., Bhuyan, P.K., Moorthy, K.K., Gogoi, M.M., Babu, S.S., Chutia, L., Ajay, P., Biswas, J., Bharali, C., Borgohain, A., Dhar, P., Guha, A., De, B.K., Banik, T., Chakraborty, M., Kundu, S.S., Sudhakar, S., Singh, S.B. (2016). Aerosol characteristics in north-east India using ARFINET spectral optical depth measurements. Atmos. Environ. 125, 461–473. https://doi.org/10.1016/j.atmosenv.2015.07.038

Qu, Z., Henze, D.K., Li, C., Theys, N., Wang, Y., Wang, J., Wang, W., Han, J., Shim, C., Dickerson, R.R., Ren, X. (2019). SO_2 emission estimates using OMI SO_2 retrievals for 2005-2017. J. Geophys. Res. 124, 8336–8359. https://doi.org/10.1029/2019JD030243

Ramachandran, S., Cherian, R. (2008). Regional and seasonal variations in aerosol optical characteristics and their frequency distributions over India during 2001-2005. J. Geophys. Res. 113, D08207. https://doi.org/10.1029/2007JD008560

Ramachandran, S., Kedia, S., Srivastava, R. (2012). Aerosol optical depth trends over different regions of India. Atmos. Environ. 49, 338–347. https://doi.org/10.1016/j.atmosenv.2011.11.017

Ramachandran, S., Kedia, S. (2013). Aerosol optical properties over South Asia from ground-based observations and remote sensing: A review. Climate 1, 84–119. https://doi.org/10.3390/cli1030084

Ramanathan, V., Crutzen, P.J., Lelieveld, J., Mitra, A.P., Althausen, D., Anderson, J., Andreae, M.O., Cantrell, W., Cass, G.R., Chung, C.E., Collins, W.D., Conant, W.C., Dulac, F., Heintzenberg, J., Heymsfield, A.J., Holben, B., Howell, S., Hudson, J., Jayaraman, A., … Valero, F.P.J. (2001). Indian Ocean Experiment: An integrated analysis of the climate forcing and effects of the great Indo-Asian haze. J. Geophys. Res. 106, 28371–28398. https://doi.org/10.1029/2001JD900133

Ramanathan, V., Chung, C., Kim, D., Bettge, T., Buja, L., Kiehl, J.T., Washington, W.M., Fu, Q., Sikka, D.R., Wild, M. (2005). Atmospheric brown clouds: Impacts on South Asian climate and hydrological cycle. Proc. Natl. Acad. Sci. 102, 5326–5333. https://doi.org/10.1073/pnas.0500656102

Randles, C.A., Silva, A.M.D., Buchard, V., Colarco, P.R., Darmenov, A., Govindaraju, R., Smirnov, A., Holben, B., Ferrare, R., Hair, J., Shinozuka, Y., Flynn, C.J. (2017). The MERRA-2 aerosol reanalysis, 1980 onward. Part I: System description and data assimilation evaluation. J. Clim. 2, 6823–6850. https://doi.org/10.1175/JCLI-D-16-0609.1

Ranjan, A.K., Patra, A.K., Gorai, A.K. (2020). Effect of lockdown due to SARS COVID-19 on aerosol optical depth (AOD) over urban and mining regions in India. Sci. Total Environ. 745, 141024. https://doi.org/10.1016/j.scitotenv.2020.141024

Ranzi, A., Porta, D., Badaloni, C., Cesaroni, G., Lauriola, P., Davoli, M., Forastiere, F. (2014). Exposure to air pollution and respiratory symptoms during the first 7 years of life in an Italian birth cohort. Occup. Environ. Med. 71, 430–436. https://doi.org/10.1136/oemed-2013-101867

Reddy, M.S., Venkataraman, C. (2002). Inventory of aerosol and sulphur dioxide emissions from India: I—Fossil fuel combustion. Atmos. Environ. 36, 677–697. https://doi.org/10.1016/S1352-2310(01)00463-0

Rodriguez-Villamizar, L.A., Magico, A., Osornio-Vargas, A., Rowe, B.H. (2015). The effects of outdoor air pollution on the respiratory health of Canadian children: A systematic review of epidemiological studies. Can. Respir. J. 22, 282–292. https://doi.org/10.1155/2015/263427

Rosenfeld, D., Lohmann, U., Raga, G.B., Dowd, C.D.O., Kulmala, M., Fuzzi, S., Reissell, A., Andreae, M.O. (2008). Flood or drought: How do aerosols affect precipitation? Science. 321, 1309–1314. https://doi.org/10.1126/science.1160606

Sadavarte, P., Venkataraman, C. (2014). Trends in multi-pollutant emissions from a technology-linked inventory for India: I. Industry and transport sectors. Atmos. Environ. 99, 353–364. https://doi.org/10.1016/j.atmosenv.2014.09.081

Satheesh, S.K., Suresh Babu, S., Padmakumari, B., Pandithurai, G., Soni V.K. (2016). Variability of

atmospheric aerosols over india, in: Rajeevan, M., Nayak, S. (Eds.), Observed climate variability and change over the Indian region. Springer, Singapore. https://doi.org/10.1007/978-981-10-2531-0_13

Schneider, P., Lahoz, W.A., van Der A, R. (2015). Recent satellite-based trends of tropospheric nitrogen dioxide over large urban agglomerations worldwide. Atmos. Chem. Phys. 15, 1205–1220. https://doi.org/10.5194/acp-15-1205-2015

Seinfeld, J.H., Pandis, S.N. (2006). Atmospheric chemistry and physics from air pollution to climate change, 2nd edition. John Wiley & Sons, Inc, New Jersey.

Sharma, S., Zhang, M., Gao, J., Zhang, H., Harsha, S. (2020). Effect of restricted emissions during COVID-19 on air quality in India. Sci. Total Environ. 728, 138878. https://doi.org/10.1016/j.scitotenv.2020.138878

Siciliano, B., Dantas, G., Cleyton, M., Arbilla, G. (2020). Increased ozone levels during the COVID-19 lockdown: Analysis for the city of Rio de Janeiro, Brazil. Sci. Total Environ. 737, 139765. https://doi.org/10.1016/j.scitotenv.2020.139765

Singh, R.P., Dey, S., Tripathi, S.N., Tare, V., Holben, B. (2004). Variability of aerosol parameters over Kanpur, northern India. J. Geophys. Res. 109, D23206. https://doi.org/10.1029/2004JD004966

Sinha, P., Nageswararao, M.M., Dash, G.P., Nair, A., Mohanty, U.C. (2019). Pre-monsoon rainfall and surface air temperature trends over India and its global linkages. Meteorol. Atmos. Phys. 131, 1005–1018. https://doi.org/10.1007/s00703-018-0621-6

Smedt, I.D., Stavrakou, T., Müller, J.F., van der A, R.J., van Roozendael, M. (2010). Trend detection in satellite observations of formaldehyde tropospheric columns. Geophys. Res. Lett. 37, L18808. https://doi.org/10.1029/2010GL044245

Soni, V.K., Pandithurai, G., Pai, D.S. (2016). Is there a transition of solar radiation from dimming to brightening over India? Atmos. Res. 169, 209–224. https://doi.org/10.1016/j.atmosres.2015.10.010

Stavrakou, T., Müller, J.F., Boersma, K.F., De Smedt, I., van der A, R.J. (2008). Assessing the distribution and growth rates of NO_x emission sources by inverting a 10-year record of NO_2 satellite columns. Geophys. Res. Lett. 35, L10801. https://doi.org/10.1029/2008GL033521

Sun, K., Zhu, L., Cady-Pereira, K., Chan Miller, C., Chance, K., Clarisse, L., Coheur, P.F., González Abad, G., Huang, G., Liu, X., Van Damme, M., Yang, K., Zondlo, M. (2018). A physics-based approach to oversample multi-satellite, multispecies observations to a common grid. Atmos. Meas. Tech. 11, 6679–6701. https://doi.org/10.5194/amt-11-6679-2018

Surl, L., Palmer, P.I., González Abad, G. (2018). Which processes drive observed variations of HCHO columns over India? Atmos. Chem. Phys. 18, 4549–4566. https://doi.org/10.5194/acp-18-4549-2018

U.S. EPA (2015). Technical Support Document EPA's 2011 National-scale Air Toxics Assessment, 2011 NATA TSD. https://www.epa.gov/sites/production/files/2015-12/documents/2011-nata-tsd.pdf

Vasilkov, A.P., Joiner, J., Oreopoulos, L., Gleason, J.F., Veefkind, P., Bucsela, E., Celarier, E.A., Spurr, R.J.D., Platnick, S. (2009). Impact of tropospheric nitrogen dioxide on the regional radiation budget. Atmos. Chem. Phys. 9, 6389–6400. https://doi.org/10.5194/acp-9-6389-2009

World Health Organization (WHO) (2013). Review of evidence on health aspects of air pollution – REVIHAAP project: Final technical report. World Health Organization.

World Health Organization (WHO) (2020a). Novel Coronavirus (2019-nCoV): Situation report, 1. World Health Organization. https://apps.who.int/iris/handle/10665/330760

World Health Organization (WHO) (2020b). Coronavirus disease (COVID-19): Situation report, 139. World Health Organization. https://apps.who.int/iris/handle/10665/332388

Xu, K., Cui, K., Young, L.H., Wang, Y.F., Hsieh, Y.K., Wan, S., Zhang, J. (2020). Air quality index , indicatory air pollutants and impact of COVID-19 event on the air quality near Central China. Aerosol Air Qual. Res. 20, 1204–1221. https://doi.org/10.4209/aaqr.2020.04.0139

Zhu, L., Jacob, D.J., Keutsch, F.N., Mickley, L.J., Scheffe, R., Strum, M., González Abad, G., Chance, K., Yang, K., Rappenglück, B., Millet, D.B., Baasandorj, M., Jaeglé, L., Shah, V. (2017). Formaldehyde (HCHO) as a hazardous air pollutant: Mapping surface air concentrations from satellite and inferring cancer risks in the United states. Environ. Sci. Technol. 51, 5650–5657. https://doi.org/10.1021/acs.est.7b01356